Applied Physics Express

LETTER

Harmonic mode-locking in an external cavity tapered diode laser with saw-toothed microstructure

Applied Physics Express 12, 102011 (2019)
https://doi.org/10.7567/1882-0786/ab3ee6

LETTER

Harmonic mode-locking in an external cavity tapered diode laser with saw-toothed microstructure

Yanjing Wang[1,2], Xin Zhang[1,2], Cunzhu Tong[1*], Lijie Wang[1], Shili Shu[1], and Lijun Wang[1]

[1]State Key Laboratory of Luminescence and Applications, Changchun Institute of Optics, Fine Mechanics and Physics, Chinese Academy of Sciences, Changchun 130033, People's Republic of China
[2]Center of Materials Science and Optoelectronics Engineering, University of Chinese Academy of Sciences, Beijing 100049, People's Republic of China

*E-mail: tongcz@ciomp.ac.cn

Received July 5, 2019; revised August 23, 2019; accepted August 27, 2019; published online September 12, 2019

In the present study, we report the passive harmonic mode-locking (HML) of the external cavity tapered semiconductor laser system with saw-toothed microstructure. The stable picosecond pulse trains were observed up to the third order HML. The mechanism behind the system was analyzed and single-pulse energy of 59 pJ with a repetition rate of 412 MHz and pulse duration of 3.9 ps was realized.

In recent years, the demand for lasers generating high-power picosecond optical pulses has increased significantly. Such lasers are widely used for precision processing of materials,[1–4] parametric oscillators pumping,[5–8] multiphoton imaging,[9–12] and supercontinuum generation.[13–15] A typical laser structure is based on optical fiber master oscillator power amplifier system that incorporates a semiconductor laser seed to generate high-power picosecond optical pulses.[16,17] To achieve this, a tunable repetition rate at the level of sub-GHz is required.[18–21] This condition is fulfilled using the technique of external cavity harmonic mode-locking (HML), a reliable solution for this kind of seed diode laser.

Certain HML approaches, such as compound-cavity mode-locking (CCM),[22–24] compound-cavity lasers incorporating distributed Bragg reflector (DBR),[25–27] and sampled grating DBR (SG-DBR)[28–30] have been proposed to attain high-performance pulse seed source. However, these methods are associated with some disadvantages. For instance, CCM requires highly accurate cleaving of the sub-cavity with a length resolution as high as a few micrometers,[22–24] which is considerably challenging to achieve. Moreover, CCM effect with DBR requires second epitaxial growth,[25–27] whereas mode-locking with SG-DBR laser requires lithography with nanoscale resolution.[28–30]

In the present study, we propose a simple and effective approach based on the tapered waveguide with saw-toothed microstructure and demonstrate the HML up to the third order with sub-GHz repetition rates. We also present the mechanism behind the proposed model. Picosecond pulse was realized and the pulse characteristics and lasing spectra were analyzed.

Figure 1 (a) shows the structure and setup of HML using a mode-locked tapered waveguide laser with saw-toothed microstructure. The saw-toothed microstructure consists of several right-angled isosceles triangles with one edge on the tapered waveguide; it plays the role of a reflector. A straight ridge waveguide applied with inverse voltage was used as the saturable absorber (SA) to lock the phase of tapered waveguide laser. The facet near the ridge waveguide was coated with a high-reflection (HR) coating, whereas the tapered side was coated with an anti-reflection coating. After fast- and slow-axes collimation, an output coupler (OC) was used to supply feedback and obtain an external cavity with the HR facet. This setup of external cavity kept the repetition rate at the level of several million Hertz, resulting in high-power pulses.

Figure 1 (b) shows the mechanism of HML based on the tapered laser having a saw-toothed microstructure. A saw-toothed microstructure forms an included angle θ with the tapered waveguide, which plays the role of a reflector. An optical pulse train with interval Δt was reflected into the cavity by the OC and subsequently reflected back by the saw-toothed microstructure. These two pulse trains in opposite directions overlap and interfere with the tapered section. Finally, a new train pulse with interval $\Delta t/n$ ($n = 1, 2, 3\ldots$) was formed.

To select the value of θ, the optical simulation was performed using finite difference time domain solutions. In the simulation, the full-flare angle was 3°, and the width of the front facet of the tapered waveguide was 6 μm. Owing to the limitation of software performance, we selected the length of the tapered waveguide as 90 μm, which did not affect the determination of the best θ value. The calculated power reflectivity at different values of θ is shown in Fig. 2(a). It can be seen that the reflectivity for $\theta = 90°$ exhibited the highest value, and therefore we selected this value for our experimental work. Figure 2(b) shows the optical field distribution of the fundamental TE_{00} mode with $\theta = 90°$ in the tapered waveguide. It can be seen that the side-wall saw-toothed microstructure reflects the optical field and enhances the energy distribution in the tapered region, which is one of the important roles of side-wall saw-toothed microstructure.

In the present work, the epitaxial structure of laser device consisted of a typical asymmetric super-large optical cavity (SLOC)[31] and was grown by metal organic chemical vapor deposition on n+ gallium arsenide (GaAs) substrate. The gain material of the laser device was two indium gallium arsenide (InGaAs) quantum wells with emission at 965 nm. The active region was embedded into an asymmetric SLOC consisting of 3.0 and 1.2 μm n- and p-type doped aluminum gallium arsenide (AlGaAs) waveguides. The cladding layers in n- and p-type doped sides were 600 nm and 550 nm $Al_{0.35}Ga_{0.65}As$, respectively. The thickness of the heavily doped GaAs for p-type Ohmic contact was 200 nm.

The total length of the fabricated tapered passive HML laser was 3020 μm, which included a ridge waveguide SA section and a tapered gain section. The SA section was 120 long and 5 μm wide. The tapered gain section had a full-flare angle of 3° and a length of 2885 μm. The waveguides

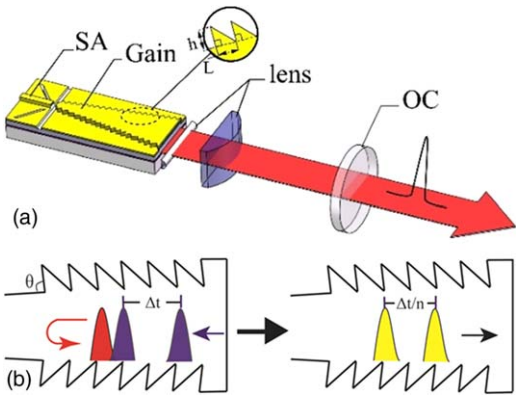

Fig. 1. (Color online) (a) Experimental setup and (b) schematic diagram of the mechanism to achieve HML pulses. HML, harmonic mode- locking; OC, output coupler, and SA, saturable absorber.

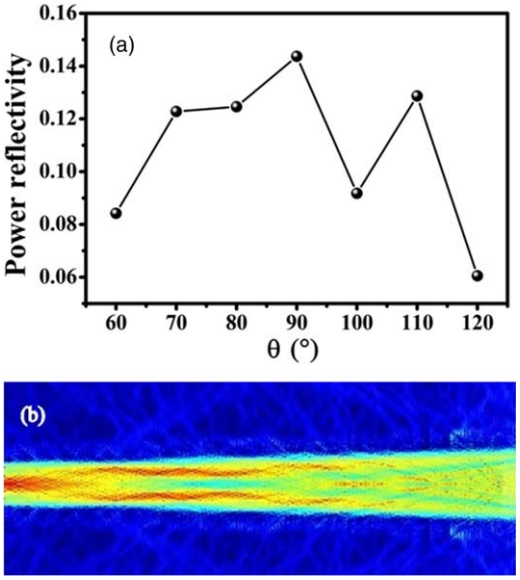

Fig. 2. (Color online) (a) Power reflectivity for different values of angle θ; θ represents the angle between the saw-toothed microstructure and the tapered waveguide. (b) The calculated optical field distribution along the cavity direction with $\theta = 90°$ (red and blue colors denote the highest and the lowest intensities, respectively).

and saw-toothed microstructure were first fabricated using inductively coupled plasma etching with a depth of 1.5 μm. The shape of the side-wall saw-toothed microstructure is a right triangle with a length (L) of 3 μm and a height (h) of 2.5 μm. Then, 15 μm wide and 400 nm deep slots were etched down to the contact layer to achieve electrical isolation between the electrodes. Simultaneously, two isolative grooves were added around the SA, with a depth greater than that of the waveguide layer. The isolative groove is used for breaking the spreading of the multi-order mode. Then, an electrical insulating layer was deposited and contact window opening was performed, followed by p-side Ti–Pt–Au contact metal deposition, substrate thinning, and n-side AuGeNi–Au metal deposition. An anti-reflection coating of 0.5% at the front facet and a HR coating of 98% at the rear facet were deposited. Finally, the laser devices were mounted n-side down on a copper heat sink using an indium solder.

In the external cavity setup as shown in Fig. 1(a), two spherical cylindrical lenses with focal lengths of 0.36 mm and 7.5 mm were used to collimate the beam in slow and fast axes, respectively. An OC with transmissivity of 67% was used for the external cavity feedback. The temperature of the laser device was stabilized to 21 °C using a Peltier cooler. The total length of the external cavity was 35 cm. The laser cavity was aligned for the lowest losses by minimizing the threshold current without reverse voltage at the SA region.

With the increase in the gain current, a stable HML was observed at a reverse voltage of SA of 3.24 V. Figure 3 shows the pulse train of different HML orders measured by Tektronix MSO5-2000. When the gain current was higher than 667 mA, a stable fundamental mode-locking pulse train could be obtained on the oscilloscope, as shown in Fig. 3(a). The fundamental repetition rate was 412 MHz, which matched well with the cavity roundtrip time of approximately 2.4 ns, indicating one pulse in one roundtrip. Continuously increasing the current of the tapered gain section to 687 mA divided the pulse into two identical pulses, which always appeared in the middle and were equal to the pulse intervals corresponding to the exactly doubled repetition rate of 824 MHz [Fig. 3(b)]. When the gain current was continuously increased to 727 mA, the stable pulse trains three times that of the fundamental repetition rate were observed as well [Fig. 3(c)].

The measured radio frequency results of the HMLs by ROHDE & SCHWARZ FSVR40 are shown in Fig. 4 and the accurate repetition rate of HML is given. When the gain current was increased to more than 667 mA, the mode-locking at 412 MHz was observed, as shown in Fig. 4(a). According to Fig. 4(b), ML operated at the second harmonic frequency of 824 MHz for the gain current between 687 and 717 mA. For the third order HML, the repetition rate was 1.236 GHz, as evident from Fig. 4(c).

Figure 5(a) shows the average output power at different gain currents. The average power of HML increased from 19 to 49 mW with the increase in the gain current. With higher order HMLs, the power shoots up. Figure 5(b) shows the dependence of the laser's pulse duration (black balls) and harmonic order (blue balls) on the gain current measured by APE GmbH pulseCheck 1200. In all cases, pulse durations were derived from the measured autocorrelation traces assuming a sech^2 pulse shape. The pulse duration increased from 3.4 to 5.8 ps with the HML orders varying from first to third. At a gain current of 707 mA, the pulse duration was

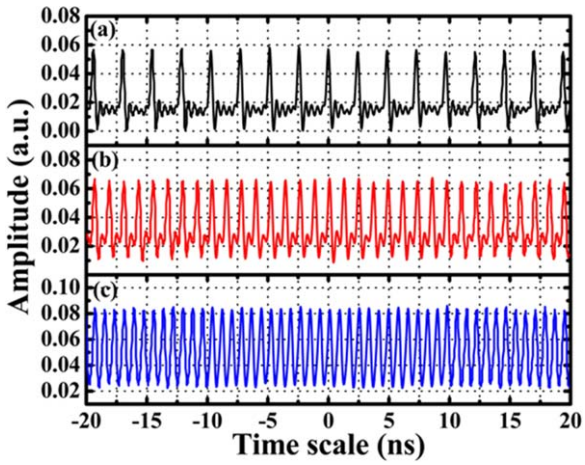

Fig. 3. (Color online) Typical pulse train of (a) the first-, (b) second-, and (c) third order HML. HML, harmonic mode-locking.

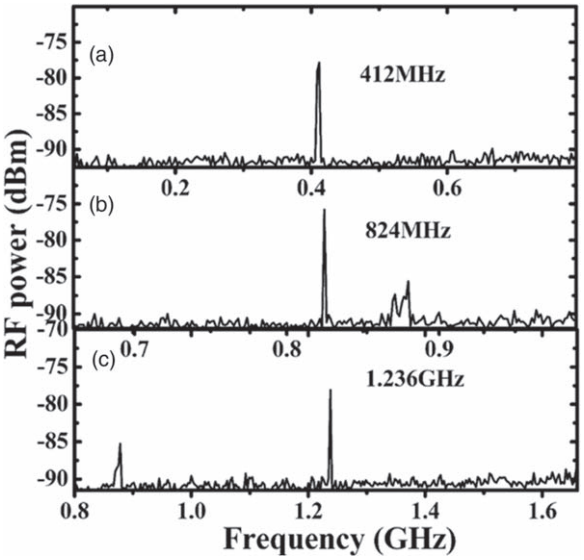

Fig. 4. RF spectrum of (a) the first order, (b) second-order, and (c) third order HML, the resolution bandwidth is 100 kHz. HML, harmonic mode-locking; RF, radio frequency.

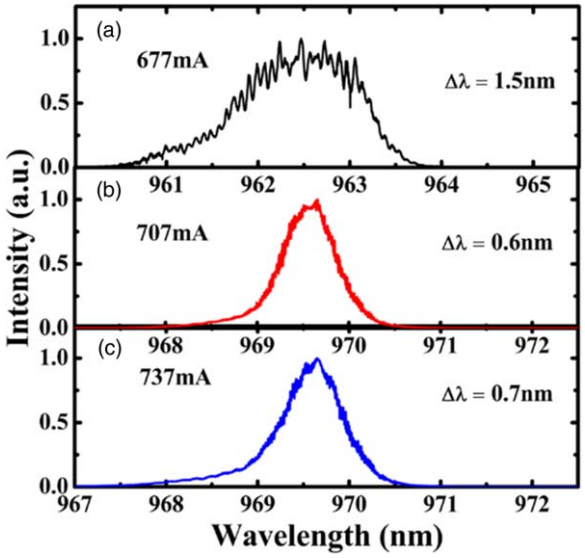

Fig. 6. (Color online) Optical spectra of the first to third order harmonic mode-locking at (a) 677 mA, (b) 707 mA, and (c) 737 mA.

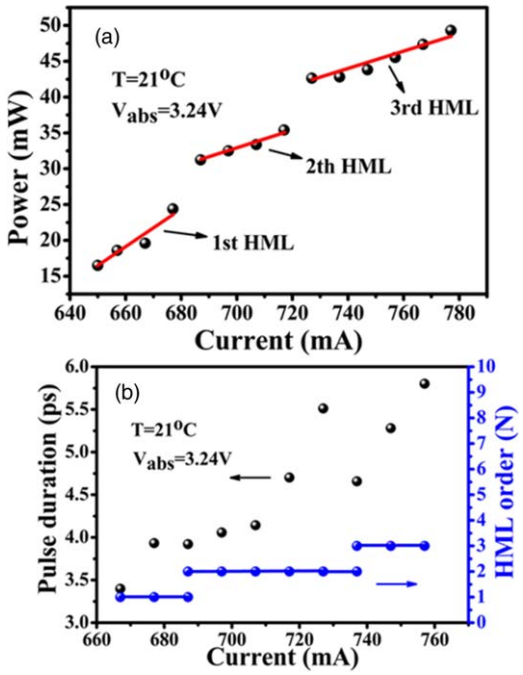

Fig. 5. (Color online) (a) Light-current characteristics and (b) pulse duration (black balls) and the harmonic order number (blue balls) for different values of gain current.

3.9 ps, which corresponded to the pulse energy of 59 pJ and a peak power of 15 W.

Figure 6 shows the optical spectra of the first- to third-order HMLs measured using Yokogawa AQ6370B. The center wavelength of the first order HML was 962.5 nm with a spectrum width of 1.5 nm for full-width at half-maximum definition [Fig. 6(a)]. With HML, the center wavelength shifted and the spectra widths became narrow. Figure 6(b) depicts the optical spectrum of the second-order HML at a gain current of 707 mA. The optical spectrum centered at 969.6 nm and the spectrum width was 0.6 nm. Figure 5(b) depicts the corresponding pulse duration of 4.1 ps. Hence, the time-bandwidth product (TBP) was estimated to be 0.79, implying the pulse was chirped. The optical spectrum of the third order HML is shown in Fig. 6(c), with corresponding pulse duration of 4.7 ps [Fig. 5(b)]. Hence, the TBP was estimated to be 1.04, which is much higher than the Fourier transform limited (∼0.315) for a sech^2 pulse shape, showing that the pulse was strongly chirped. The chirps in pulses generated from the passively mode-locked laser diodes are usually caused by self-phase modulation effects in the gain and absorber sections,[32,33] resulting from the interactions between the gain and absorption saturation mechanisms.

In conclusion, we demonstrated a passive HML operation using a side-wall saw-toothed micro-structure in external cavity semiconductor lasers. Compared with other reported devices, our laser system exhibited simplified fabrication. The maximum single-pulse energy reached up to 59 pJ, and the peak power of 15 W with pulse duration of 3.9 ps was realized. Based on these findings, we believe these results will contribute to the development of HML diode lasers.

Acknowledgments This work was supported by the National Natural Science Foundation of China (Nos. 61774153, 61774156, 61790584, and 61761136009), the International Science Technology Cooperation Program of the Chinese Academy of Sciences (No. 181722KYSB20160005), and Jilin Provincial Foundation (Nos. 20180519024JH and 20190302053GX).

ORCID iDs Yanjing Wang https://orcid.org/0000-0002-7435-8246

1) S. H. Park, D. Y. Yang, and K. S. Lee, Laser Photonics Rev. **3**, 1 (2009).
2) K. Sugioka and Y. Cheng, Light: Sci. Appl. **3**, e149 (2014).
3) M. Malinauskas, A. Žukauskas, S. Hasegawa, Y. Hayasaki, V. Mizeikis, R. Buividas, and S. Juodkazis, Light: Sci. Appl. **5**, e16133 (2016).
4) S. Toriyama, V. Mizeikis, and A. Ono, Appl. Phys. Express **12**, 015004 (2019).
5) A. Robertson, M. E. Klein, M. A. Tremont., K. J. Boller, and R. Wallenstein, Opt. Lett. **25**, 657 (2000).
6) F. Kienle, P. S. Teh, D. Lin, S. Alam, J. H. V. Price, D. C. Hanna, D. J. Richardson, and D. P. Shepherd, Opt. Express **20**, 7008 (2012).
7) F. Kienle, D. Lin, S. Alam, H. S. S. Hung, C. B. E. Gawith, H. E. Major, D. J. Richardson, and D. P. Shepherd, J. Opt. Soc. Am. B **29**, 144 (2012).
8) W. Tian, Z. Wang, J. Zhu, and Z. Wei, Opt. Express **24**, 29814 (2016).
9) M. Kuramoto, N. Kitajima, H. Guo, Y. Furushima, M. Ikeda, and H. Yokoyama, Opt. Lett. **32**, 2726 (2007).

10) E. P. Perillo, J. W. Jarrett, Y. L. Liu., A. Hassan, D. C. Fernée, J. R. Goldak, A. Bonteanu, D. J. Spence, H. C. Yeh, and A. K. Dunn, Light: Sci. Appl. **6**, e17095 (2017).
11) C. Lefort, J. Phys. D: Appl. Phys. **50**, 423001 (2017).
12) K. Guesmi et al., Light: Sci. Appl. **7**, 1 (2018).
13) W. Yang, B. Zhang, K. Yin, X. Zhou, and J. Hou, Opt. Express **21**, 19732 (2013).
14) Y. Nomura, H. Kawagoe, Y. Hattori, M. Yamanaka, E. Omoda, H. Kataure, Y. Sakakibara, and N. Nishizawa, Appl. Phys. Express **7**, 122703 (2014).
15) M. Yamanaka, H. Kawagoe, and N. Nishizawa, Appl. Phys. Express **9**, 022701 (2016).
16) H. Yokoyama, H. Guo, T. Yoda, K. Takashima, K. Sato, H. Taniguchi, and H. Ito, Opt. Express **14**, 3467 (2006).
17) H. Yokoyama, A. Sato, H. Guo, K. Sato, M. Mure, and H. Tsubokawa, Opt. Express **16**, 17752 (2008).
18) K. K. Chen et al., Opt. Express **18**, 5426 (2010).
19) F. Kienle, K. K. Chen, S. Alam, C. B. E. Gawith, J. I. Mackenzie, D. C. Hanna, D. J. Richardson, and D. P. Shepherd, Opt. Express **18**, 7602 (2010).
20) Y. Kusama, Y. Tanushi, M. Yokoyama, R. Kawakami, T. Hibi, Y. Kozawa, T. Nemoto, S. Sato, and H. Yokoyama, Opt. Express **22**, 5746 (2014).
21) J. Lopez, K. Mishchik, G. Mincuzzi, E. Audouard, E. Mottay, and R. Kling, J. Laser Micro/Nanoen **12**, 296 (2017).
22) D. A. Yanson, M. W. Street, S. D. McDougall, I. G. Thayne, J. H. Marsh, and E. A. Avrutin, IEEE J. Quantum Electron. **38**, 1 (2002).
23) L. Hou, M. Haji, R. Dylewicz, P. Stolarz, B. Qiu, E. A. Avrutin, and A. Bryce, Opt. Lett. **35**, 3991 (2010).
24) L. Hou, E. A. Avrutin, M. Haji, R. Dylewicz, A. C. Bryce, and J. H. Marsh, IEEE J. Sel. Top. Quantum Electron. **19**, 1100409 (2013).
25) S. Arahira, S. Oshiba, Y. Matsui, T. Kunii, and Y. Ogawa, Opt. Lett. **19**, 834 (1994).
26) S. Arahira, Y. Matsui, and Y. Ogawa, IEEE J. Quantum Electron. **32**, 1211 (1996).
27) U. Bandelow, R. Mindaugas, A. Vladimirov, B. Hüttl, and R. Kaiser, Opt. Quantum Electron. **38**, 495 (2006).
28) L. Hou, M. Haji, and J. H. Marsh, Opt. Lett. **38**, 1113 (2013).
29) L. Hou, M. Haji, and J. H. Marsh, Opt. Express **22**, 21690 (2014).
30) L. Hou, S. Tang, B. Hou, S. Liang, and J. H. Marsh, IEEE J. Sel. Top. Quantum Electron. **24**, 1102508 (2018).
31) T. Wang, C. Tong, L. Wang, Y. Zeng, S. Tian, S. Shu, J. Zhang, and L. Wang, Appl. Phys. Express **9**, 112102 (2017).
32) D. J. Derickson, R. J. Helkey, A. Mar, J. R. Karin, J. G. Wasserbauer, and J. E. Bowers, IEEE J. Quantum Electron. **28**, 2186 (1992).
33) H. Wang, L. Kong, A. Forrest, D. Bajek, S. E. Haggrtt, X. Wang, B. Cui, J. Pan, Y. Ding, and M. A. Cataluna, Opt. Express **22**, 25940 (2014).